Cross-plane Conductance through a Graphene/Molecular Monolayer/Au Sandwich

Li, Bing; Albrecht, Tim; Famili, Marjan; Pensa, Evangelina; Grace, Iain Mark; Long, Nicholas J.; Lambert, Colin; Cohen, Lesley

DOI:
10.1039/C8NR06763E

Nanoscale

Accepted Manuscript

This article can be cited before page numbers have been issued, to do this please use: B. Li, M. Famili, E. Pensa, I. M. Grace, N. J. Long, C. Lambert, T. Albrecht and L. Cohen, *Nanoscale*, 2018, DOI: 10.1039/C8NR06763E.

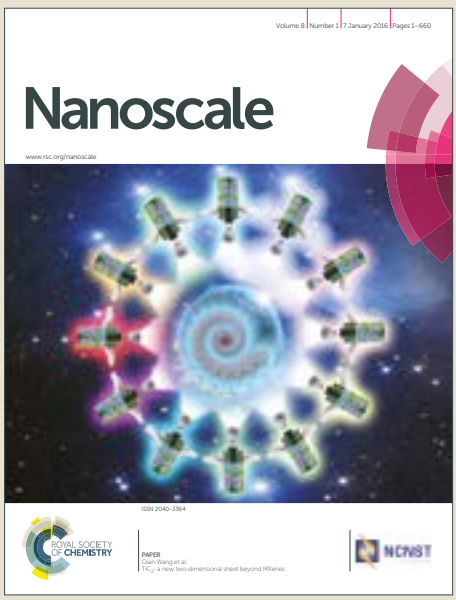

ROYAL SOCIETY OF CHEMISTRY

rsc.li/nanoscale

View Article Online
DOI: 10.1039/C8NR06763E

Nanoscale

ARTICLE

Cross-plane Conductance through a Graphene/Molecular Monolayer/Au Sandwich

Received 00th August 2018,
Accepted 00th January 20xx

DOI: 10.1039/x0xx00000x

www.rsc.org/

Bing Li[a, †, *], Marjan Famili[b, †], Evangelina Pensa[c], Iain Grace[b], Nicholas J. Long[c], Colin Lambert[b], Tim Albrecht[c, &], Lesley F. Cohen[a]

Abstract: The functionalities offered by single-molecule electrical junctions have yet to be translated into monolayer or few-layer molecular films, where effective and reproducible electrical contact represents one of the challenging bottlenecks. Here we take a significant step in this direction by demonstrating that excellent electrical contact can be made to a monolayer biphenyl-4, 4'-dithiol (BPDT) molecular film, sandwiched between gold and graphene electrodes. This sandwich device structure is advantageous, because the current flows through the molecules to the gold substrate in a 'cross-plane' manner, perpendicular to the plane of the graphene, yielding high-conductance devices. We elucidate the nature of cross-plane graphene/molecule/Au transport using quantum transport calculations and introduce a simple analytical model, which captures generic features of the current-voltage characteristic. Asymmetry in junction properties results from the disparity in electrode electrical properties, the alignment of the BPDT HOMO-LUMO energy levels and the specific characteristics of the graphene electrode. The experimental observation of scalability of junction properties within the junction area, in combination with a theoretical description of the transmission probability of the thiol-graphene contact, demonstrate that between 10%-100% of the molecules are contacted to the electrodes, which is several orders of magnitude greater than achieved to date in the literature.

1. Introduction

Single-molecule electronic devices, have been widely studied as a possible route to drive Moore's Law to the next level of sub-10 nm electronics.[1-3] Various methods have been used to explore electron transport characteristics of molecular structures, including scanning tunnelling microscopy,[4] mechanical break junctions and eutectic gallium–indium junctions.[5, 6] At the single-molecule level, quantum interference effects are particularly evident and open up many possibilities for functional design of electronic and thermoelectric devices. [7, 8] However, for many of these applications, those features that are attractive at the single molecular level, should be scaled up to self-assembled molecular (SAM) films without losing the single-molecule functional advantages through inhomogeneous broadening, intermolecular interactions and defects.[9] For the study of vertical transport through SAM layers, direct evaporation of a metal top electrode onto organic molecules has not proved feasible as it leads to short circuits via pinholes in the organic layer. Various attempts have been made to overcome this problem, such as the addition of a conducting protective layer between the organic molecules and the top electrode.[10-12] Also, a mechanically transferred electrode has recently been reported to replace the direct formation of the metal electrode onto the SAM.[13] Nevertheless, a widespread observation is that scale up of junctions to practical device dimensions produce irreproducible properties that vary with the electrode choice. Moreover, it is observed that the (apparent) resistance per molecule increases by up to a factor of 10^8 in large area junctions (consisting of 10^3 to 10^8 molecules) .[14-16] These observations strongly suggest that for most large scale junction architectures the number of molecules that make electrical contact to the electrode are fractions of a percent and the contacting becomes increasingly inefficient as the junction area increases. In addition, in an attempt to mitigate this problem, the unique properties of the organic molecules can be lost by the addition of a protective layer, and/or the minimum thickness of the transferred metal forming the top contact may limit miniaturization of the molecular devices. Graphene, as a monolayer of sp^2 - hybridised carbon atoms,[17] offers an opportunity in this regard as it presents electron mobility of up to 10^6 cm^2V^{-1} s^{-1} at room temperature,[18] ultralow resistivity, [19] ultrahigh breaking strength of 1 TPa and a controllable doping level.[20] However to date, there have only been a few reports in the literature using

[a] The Blackett Laboratory, Imperial College London, South Kensington Campus, London SW7 2AZ.
[b] Physics Department, Lancaster University, Lancaster LA1 4YB, UK.
[c] Department of Chemistry, Imperial College London, South Kensington Campus, London SW7 2AZ, UK.
*Corresponding Author: Email: b.li@imperial.ac.uk; Tel: +44(0)7831657979
†Bing Li and Marjan Famili contributed equally to this work.
&Present address: University of Birmingham, School of Chemistry, Edgbaston Campus, Birmingham, B15 2TT, UK.
Electronic Supplementary Information (ESI) available: ESI has been uploaded separately.

View Article Online
DOI: 10.1039/C8NR06763E

low-dimensional carbon based materials as electrodes for solid state vertical transport devices.[21] In particular graphene and its derivative oxide have been found to be a useful electrode.[22] However, a limitation is that such oxide flakes cannot be easily scaled up to large area arrays of nano-patterned devices in a controllable way (due to the randomly distributed oxygen moieties) or their studies focus on the impact of different molecular orientation and structure rather than electrical contacts.[23]

Our aim in the present work is to study the tunnelling current through a SAM layer sandwiched between two electrodes and to demonstrate that excellent electrical contact can be achieved. For this purpose, we sandwich a monolayer biphenyl-4, 4'-dithiol (BPDT) molecular film, between gold and graphene electrodes (see Figure 1 (a) and (b)) and measure the cross-plane current flowing perpendicular to the plane of the graphene, through the SAM and the gold. The aim of this study is to understand the fundamental characteristics of such graphene/SAM/Au devices. We chose BPDT for the molecular layer, because the single-molecule electrical conductance of BPDT has been measured (here and previously) and calculated and it is known to form a tightly packed SAM on gold.[24, 25]

In addition to detailed characterisation of the graphene/BPDT/Au sandwiches, we carry out calculations of their electrical conductance using density functional theory (DFT) combined with quantum transport theory. We also develop a simple analytical model, which captures the key features of room-temperature transport through such devices and enables qualitative understanding of device characteristics.

2. Experimental

2.1 STM Measurement

The conductance of Au/BPDT/Au system were measured by STM current-distance (I(s)) technique in air, with an Agilent 5100 STM operated using Pico View 1.14.[26] For these experiments a low-density layer of BPDT was prepared and then repeatedly probed by approaching and retracting the STM tip while recording the tunnelling current. Typically, this yielded a mixture of I(s) traces with and without molecular signatures, which then needed to be separated. After vector-based classification and clustering,[27, 28] we extracted a BPDT-related sub-population in the data. STM tips were fabricated by electrochemical etching of 0.25 mm wire (99.9999%, Good Fellow) in HCl / EtOH via the method of Wang et al.[29] See SI. 1 for further details.

2.2 Cyclic voltammograms (CVs)

CVs were recorded with a CHI760C potentiostat (CH Instruments, United States). A conventional three-electrode cell was employed with a Pt coil as counter electrode and a Ag/AgCl (sat) reference electrode. The Au (111) working electrode was modified with BPDT and the electrolyte degassed with Ar for at least 20 minutes before the measurement. An Ar atmosphere was maintained throughout. CVs were collected at room temperature (~25 °C) in 0.1 M NaOH aqueous solution. The potential was scanned from -0.3 V to -1.3 V at 0.1 V s^{-1}.

2.3 Device Fabrication

Fabrication of electronics and selective immobilisation of SAM were achieved using standard photolithograph process. Monolayer chemical vapour deposited (CVD) graphene was purchased from Graphenea (Spain) and transferred following the wet transfer procedures (as detailed in SI. 2). All the other chemicals, such as BPDT, ammonium persulfate and Poly (methyl methacrylate) (PMMA), etc. at biochemical grade were purchased from Sigma Aldrich (Dorset, UK).

2.4 Device Characterisation

The vertical transfer characteristics of the graphene/BPDT/Au junction were characterized using a home designed four-probe measurement system, as shown in Figure 1 (a). The dimension of graphene/BPDT/Au junction varies from 6 x 6 µm to 18 x 18 µm. Both the current and the first derivative of the current with respect to the voltage were directly recorded with an AC modulation bias of 10 mV at a frequency of 23 Hz.

Non-contact Kelvin probe force microscopy (KFM) was used to analyse the local work function and the topography of the graphene/BPDT/Au junction, directly correlating the two. Measurements were performed with a Pointprobe-plus electrical force microscopy tip (tip and detector side are coated with Pt/Ir, resonant frequency 45 - 115 kHz, k = 0.5 – 9.5 N/m). All KFM scans were conducted with a drive amplitude of 3746 mV and a lift height of 25 nm. A confocal scanning Raman microscope (WiTec Alpha 300 system) with 633 nm excitation and a 100 x objective (0.9 NA) was used to characterise the quality and the doping condition of transferred CVD graphene.

2.5 Theoretical Calculations

To gain insight into the transport properties of graphene/molecule/Au junctions, the geometry of the isolated molecule was optimised using the SIESTA implementation of density DFT method.[30] The geometry of each contact (BPDT with gold and BPDT with graphene), was optimised in the vicinity of a Au (111) surface and a graphene sheet separately. Thiol anchor groups bind to gold by losing the hydrogen and forming a covalent bond. Finally, a system with Au/BPDT/Au contact and graphene/BPDT/Au contact was constructed and the geometry of the system was optimised using the same method. The mean field Hamiltonian obtained from DFT, was combined with our quantum transport calculation code, GOLLUM to calculate the Green's function $G^r(E)$ in the presence of the electrodes.[31] The transmission coefficient $T_e(E)$ of electrons of energy E passing from the graphene to gold electrodes is calculated using $T_e(E) = \mathrm{Trace}[(G^r(E)\Gamma_S(E)G^{r\dagger}(E)\Gamma_D(E)]$ where $\Gamma_{S,D}(E) = i(\Sigma_{S,D}(E) - \Sigma_{S,D}{}^{\dagger}(E))$ is the self-energy due to the contact

View Article Online
DOI: 10.1039/C8NR06763E

between the molecule and the electrodes. More details of the theoretical method are provided in SI. 3.

3. Results and Discussion

First, we studied the single-molecule conductance of Au/molecule/Au junctions by analysing the distance-dependent tunneling current (I (s) traces) at a low coverage BPDT/Au (111) samples. Figure S1 (a) in Section 1 of Supplementary Information (SI. 1) shows the typical I(s) traces with (red) and without (black) molecular junction formation. The statistical analysis of traces containing plateaus is shown in Figure S1 (b and c). A most probable current value of 0.91 nA (equivalent to 1.82 nS) was found, in good agreement with the conductance value obtained by Haiss et al using the I (t) method (1.65 nS).[32] This is slightly lower than the value of 13.2 nS determined Mishchenko et al.,[33] which was however recorded in a solvent environment (1:4 (v/v) mixture of tetrahydrofuran/mesitylene) using the STM break-junction technique. Hence, the difference in the observed values was not unexpected.

Details of the steps of our macroscopic junction fabrication are presented in the SI. 2. To characterise precisely the conductance across graphene/BPDT/Au sandwiches, individual devices are designed in a four-probe configuration. The horizontal bottom electrode is made of Cr (2 nm) /Au (60 nm) on top of SiO_2/Si substrate, while the top graphene electrode is located between two gold contacts. The current imposed between one pair of graphene/Au arms and the voltage drop is measured across the other pair, as shown in Figure 1 (a).

Due to the π – π interaction between parallel benzene rings in BPDT molecules, the molecular layer is packed tightly onto the surface of gold electrode, rendering short-circuit between the graphene and gold electrodes less likely, as shown in Figure 1 (b). To model the flow of electrons from the gold electrode, through BPDT to the planar graphene electrode, Figure 1 (c) shows a unit cell of the system analysed using density functional theory (DFT). Each unit cell contains a single BPDT molecule and the whole structure is repeated periodically. All electronic properties of the system is obtained by summing over k-points in the plane of the graphene (The details of the theoretical approach are given in SI. 3).

Figure 1 (d) shows the measured current-voltage (I-V) characteristic of an 18 × 18 μm^2 graphene/BPDT/Au device, Figure 1 (e) presents the corresponding differential conductance dI/dV and Figure 1 (f) demonstrates how the zero bias conductance varies with junction width. The scaling is close to that expected from the variation of the junction area, which strongly suggests a rather uniform connectivity of molecules to the graphene top contact particularly for the smaller junctions. The zero-bias conductance of the 18 × 18 μm^2 junction is estimated to be $G_{SAM} \approx 3 \times 10^{-3}$ S (the value of conductance at V=0 in Figure 1(e)). To obtain the average zero-bias conductance per molecule G_M of the SAM, we first estimate the number of molecules (N) in the film and then write, $G_M = G_{SAM}/N$.

To this end, we carried out cyclic voltammetry analysis, which yielded a charge density of $(62 \pm 2)\cdot 10^{-6}$ C·cm^{-2} (as detailed in SI. 1). Therefore, the corresponding number of molecules per unit area is,

$$x = \frac{(62\pm2)\times10^{-6}\ \text{C·cm-2}}{1.602\ \times 10^{-19}\ \text{C}} = (3.75\sim4.00)\times 10^{6}(\mu\text{m})^{-2} \qquad (1)$$

Since the area of the SAM is 18 × 18 μm^2, the total number of molecules is N = (1.2 ~ 1.3) × 10^9 and therefore $G_M = G_{SAM}/N$ = (2.3 ~ 2.5) × 10^{-3} nS. Ideally, we would like to compare this with a direct measurement of the single-molecule conductance of BPDT in a single-molecule graphene/BPDT/Au device. Unfortunately, such measurement is not straightforward: in the absence of a covalent BPDT/graphene interaction, this would most likely require a graphene-based (flat) 'tip' to contact an individual BPDT molecule immobilised on gold. When both electrodes are gold, the measured conductance of a single BPDT molecule obtained by STM is 1.82 nS under ambient conditions (as detailed in SI. 1). However, the DFT modelling (see Figure 2 (a)) predicts that the conductance of a single BPDT molecule calculated between gold and graphene electrodes should be approximately a

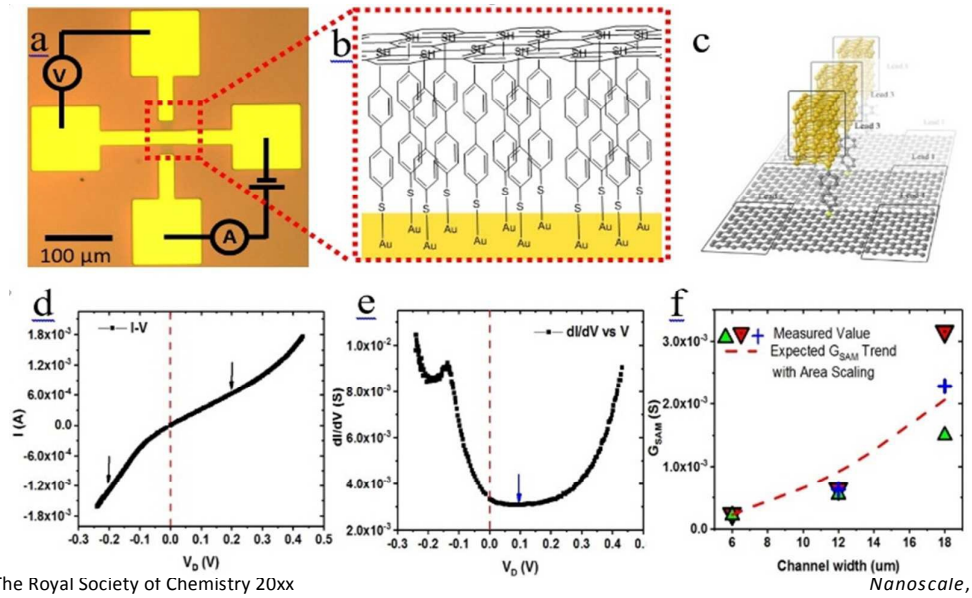

Figure 1. (a) Optical image (graphene is shown as light grey colour) and (b) cross-section schematic illustration of the vertical transport device. (c) Graphene/BPDT/Au model used for calculations. Representative (d) I-V and (e) dI/dV vs V characteristics of the vertical transport device (V=0 indicated by red dash line and offset of the minimum differential conductance indicated by the blue arrow). (f) The experimentally determined zero bias conductance (G_{SAM}) versus junction width. The red dash curve is a guide to show the expected trend of G_{SAM} with junction area assuming 100% coverage.

View Article Online
DOI: 10.1039/C8NR06763E

factor of 10^2~ 10^3 lower than this value, which leads to a calculated G_M of $G_M \approx (10^{-2} \sim 10^{-3})$ nS.[‡] Comparison with our measured value of $G_M = (2.3 \sim 2.5) \times 10^{-3}$ nS as well as the approximate scaling of the conductance with junction area (shown in Figure 1(f)), leads us to the conclusion, in contrast to many previous results on large area junctions, that between 10% and 100% of the molecules in our SAM are electrically-connected to the electrodes.

To understand the asymmetry in the I-V characteristic of Figure 1 and offset of the minimum differential conductance (indicated by the blue arrow), we now introduce a generic model of cross-plane, single-molecule phase-coherent tunnelling in the presence of graphene electrodes (shown in Figure 2 (b)), which captures the interplay between the closest energy level on the molecule and the Dirac point of the graphene.

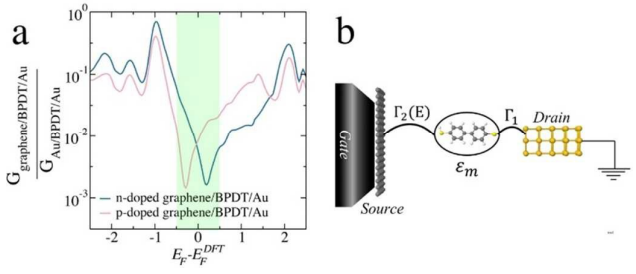

Figure 2: (a) The predicted room-temperature electrical conductance of a n-doped graphene/BPDT/Au junction (blue) and a p-doped graphene/BPDT/Au (pink), divided by the room temperature single-molecule conductance of the Au/BPDT/Au junction. (See SI. 3 for individual conductance curves). The predicted ratio depends on the doping of the graphene and on the precise location of the Fermi energy (E_F) relative to the frontier orbitals of the molecule. However, over a range of such values in the vicinity of the DFT-predicted Fermi energy (shaded in Figure 2 (a)) the ratio varies from 10^{-2} to 10^{-3}. (b) Overview of the parameters involved in the generic model where $\Gamma_{1,2}$ are level broadening due to contact with the source and drain and Γ_m is maximum energy of the molecular orbital.

To describe this interplay, we recall the Breit-Wigner formula for the transmission coefficient *T(E)* describing electrons of energy E passing from a source to a drain via a single molecular energy level.[34]

$$T(E) = \frac{4\Gamma_1\Gamma_2}{(E-\varepsilon)^2+(\Gamma_1+\Gamma_2)^2} \quad (2)$$

In this expression, Γ_1 and Γ_2 are the level broadening due to contact with the source 1 and drain 2, while ε is the energy of the molecular orbital, shifted slightly by the real part of the self-energy due to the contacts. Clearly, when $E = \varepsilon, T(E)$ achieves a maximum value of

$$T_{max} = \frac{4\Gamma_1\Gamma_2}{(\Gamma_1+\Gamma_2)^2}$$

and for a symmetric junction where $\Gamma_1 = \Gamma_2, T_{max} = 1$. The quantity Γ_1 involves a product of the local density of states in the source electrode, the matrix element coupling the molecular orbital to the source and the amplitude of the molecular orbital in the vicinity of the contact to the source. The quantity Γ_2 involves corresponding quantities evaluated at the drain. If the source is gold, whose the local density of states is almost energy independent on the scale of the level broadening and k_BT, then Γ_1 is approximately independent of energy. On the other hand if the drain is graphene, whose local density of states is reduced near the Dirac point, Γ_2 is energy dependent and has a minimum at the Dirac point. Therefore in a graphene/molecule/Au junction Γ_2 will depend on both the source-drain voltage V_D and (in a three-terminal device) on the applied gate voltage V_g. In general, ε will also depend on these voltages therefore for a graphene/BPDT/Au device, the transmission per molecule will take the form

$$T(E, V_g, V_D) = \frac{4\Gamma_1\Gamma_2(E, V_g, V_D)}{\left(E - \varepsilon(V_g, V_D)\right)^2 + \left(\Gamma_1 + \Gamma_2(E, V_g, V_D)\right)^2} \quad (3)$$

Where Γ_1 and $\Gamma_2(E, V_g, V_D)$ are the level broadenings. In a pristine monolayer device, Γ_2 would vanish at the Dirac point, but in a real device, due to inhomogeneous broadening, Γ_2 will not vanish precisely. Therefore we assume an energy dependence of the form

$$\Gamma_2(E, V_g, V_D) = \Gamma_0 + \alpha[E - E_{Dirac}]^z \quad (4)$$

In this equation the exponent z characterizes the energy dependence of the average density of states in the graphene, whose spatially-averaged Dirac point is E_{Dirac}. Since the latter can be tuned by both V_D and V_G , we assume a simple linear dependence

$$E_{Dirac} - E_F^{Gold} = E_0^{Dirac} - \gamma_D|e|V_D - \gamma_G|e|V_G \quad (5)$$

and similarly we write for the location of the molecular orbital relative to the Fermi energy of gold,

$$\varepsilon - E_F^{Gold} = \varepsilon_m - \beta_D|e|V_D - \beta_G|e|V_g \quad (6)$$

Where $\beta_D, \beta_G, \gamma_D$ and γ_G are the lever arms which depend on the geometry of the device.

If $\gamma_D = 1$ and V_G=0, then adjusting V_D does not change the charge on the graphene, whereas if $\gamma_D < 1$, the graphene acquires charge when V_D is non-zero. Since the molecule is strongly bound to the gold and very weakly bound to the graphene, the energy levels of the molecule are less affected by the source-drain voltage and therefore in what follows we assume $\beta_D = 0$. The absence of an electrostatic gate in our experiments is reflected in the model by choosing $\beta_G = 0$ and $\gamma_G = 0$. The current is then given by,

$$I(V_g, V_D) = I_0 \int_{E_F^{Gold}}^{E_F^{Gold} - |e|V_D} T(E, V_g, V_D)\,(|e|V_D)\,dE \quad (6)$$

where $I_0 = 2e/h$. This means that a Dirac point entering the integration interval would appear as a dip in the $\frac{dI}{dV}$ curve and the position of the Lorentzian (equation 3) relative to the Dirac point would create asymmetry in the $\frac{dI}{dV}$ (see SI. 3 for a more detailed explanation).

View Article Online
DOI: 10.1039/C8NR06763E

As shown in Figure 3, the asymmetry and dip in $\frac{dI}{dV}$ can appear in four different forms depending on the doping of the graphene and whether the transport is HOMO or LUMO dominated (ie. if E_F^{Gold} lies closest to the HOMO or closest to the LUMO), and if the graphene is electron doped the dip will appear at negative bias voltages. For systems with p-doped graphene, it appears at positive bias voltages.

The broad minimum in the experimental differential conductance plot Figure 1 (e) suggests that there is a distribution of Dirac points within the device, associated with inhomogeneities in the doping. To simulate this effect in the modelling, we average twenty differential conductance plots (light grey in Figure 4 (a)) with slightly different Dirac points, whose average yields the red curve in Figure 4 (a). The fitted parameters in the red curve of Figure 4 (a) suggest that in the experiment, graphene is overall p-doped and transport is LUMO dominated.

To check if this is consistent with the film properties, we performed Kelvin Force microscopy (KFM) and RAMAN spectroscopy measurements to determine the doping of the graphene in device IA3 (differential conductance shown in Figure 4 (b)). Figure 4 (c) shows the work function image of the graphene/BPDT/Au junction area (blue-ish square). From this image, it is clear that the graphene electrode over the BPDT/Au area is differently doped with respect to the graphene on the bare SiO_2 surface. Within the junction area, the graphene lying on BPDT shows a distribution of surface properties. The specific patterns are attributed to the surface arrangement of the BPDT molecules after the solvent drying process. The blurry edges between electrodes and SiO_2 are attributed to surface charging on the insulating SiO_2 substrate.

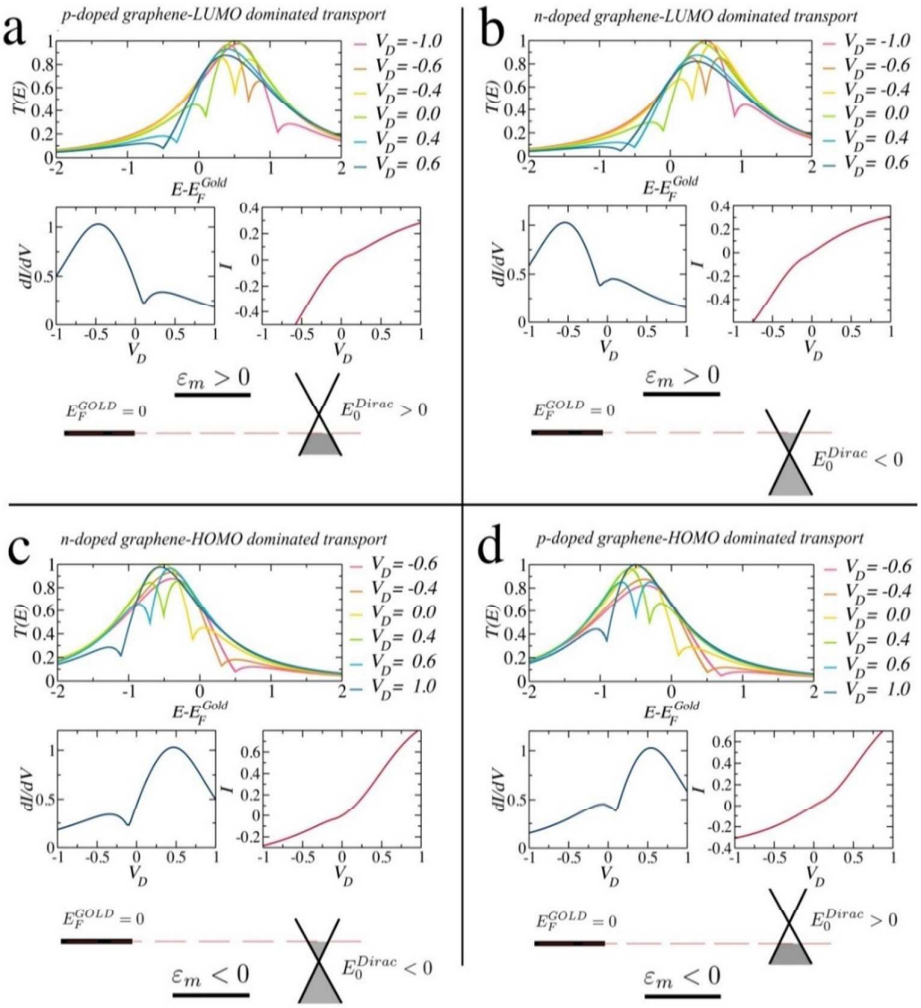

Figure 3. Four possible scenarios for the dip and asymmetry in dI/dV curve of graphene/BPDT/Au devices. The transport and graphene are (a) LUMO and p-doped (E_{Dirac}=0.1 and ε_m=0.5) (b) LUMO dominated, n-doped (E_{Dirac}=-0.1 and ε_m=0.5) (c) HOMO dominated, n-doped (E_{Dirac}=-0.1 and ε_m=-0.5) and (d) HOMO dominated, p-doped (E_{Dirac}=+0.1 and ε_m=-0.5). For all four scenarios Γ_0=0.1, α=1 and z=1. In each quadrant, the transmission coefficient $T_e(E)$ vs energy $E\text{-}E_F^{Gold}$ (the energy, relative to the fermi energy of the gold) is plotted at various drain voltages V_D (top graph), the differential conductance (dI/dV) and the current (I) versus the drain voltage are plotted (middle graphs left and right, respectively) and a schematic showing the position of the Fermi energy of the gold relative to graphene (bottom diagram).

View Article Online
DOI: 10.1039/C8NR06763E

Statistical analysis of the work function difference within the junction areas is compared to that of the graphene on SiO_2 presented in Figure 4 (d). The centre of the distribution shifts negatively indicating that graphene is more p-doped when transferred onto BPDT in comparison with graphene on SiO_2. The KFM images show the difference in work function with respect to the KFM tip's work function; the absolute values of the peak positions do not provide quantitative information, but since they are offset by the same amount, the difference between the positions of the two peaks is a meaningful quantity. Notably, CVD graphene under ambient conditions on SiO_2, is always p-doped. This is due to the charge transfer to the substrate as well as adsorption of water molecules and other contaminations from air, which act as the hole dopants.[35] In these vertical transport devices, graphene becomes more heavily p-doped when it is transferred onto BPDT, attributed to the combined influence of the BPDT molecules and the gold electrode at the far end of the graphene strip. [36]

Raman spectroscopy analysis is provided in Figure 4 (e) and (f). The white horizontal bar in Figure 4 (e) is a gold bottom electrode, whilst the darker grey square is the cross-plane BPDT-based junctions. Raman spectroscopy has been carried out across a similar area including graphene on BPDT (outlined as black dash line) and graphene on bare SiO_2 (outlined as red dash line). The position of G band positively shifts from 1583 cm^{-1} to 1584 cm^{-1}, when graphene is doped by BPDT/Au stack. Positively shifted peaks indicate the graphene is p-doped as the theoretical model predicts. In addition to the shifted distribution centre, the full-width half-maximum (FWHM) of the distribution characteristics have also increased, indicating a more dispersed and inhomogeneous doping condition with the effect from BPDT/Au stack underneath.[30]

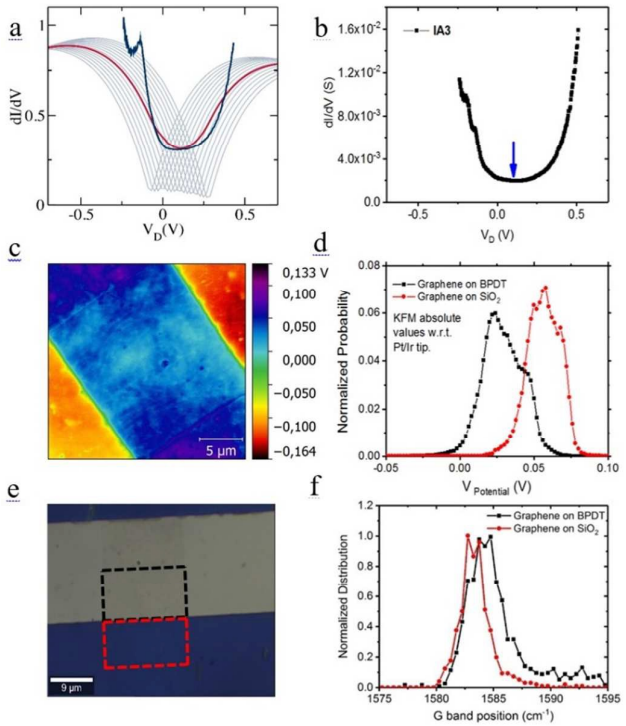

Figure 4 (a) The theoretical model (red) fit to the experimental dI/dV (blue) for the parameter $\Gamma_0 = 0.003, \alpha = 1, \gamma_0 = 0.002, \gamma_1 = 1, \gamma_d = 1, \varepsilon_m = 0.1$ and $-0.1 < E_0^{Dirac} < 0.4$. (b) The differential conductance characteristics of IA3 (minimum indicated by blue arrows). (c) KFM work function mappings of device IA3 with respect to the gold tip. (d) The corresponding statistical analysis of the work function across the junction area on BPDT of IA3 as well as one of the areas where graphene lies on the SiO2. (e) Optical images of the Raman mapped graphene areas on IA3. (f) Corresponding statistical analysis of G band position.

In addition to the analytical model of equation (3), we performed DFT-based modelling of the geometry-optimised structure shown in Figure 1 (c), which is periodic in the transverse direction, using a combination of the DFT code SIESTA and the quantum transport code GOLLUM (See SI. 3 for more details).[31, 37] At zero bias, Figure 5 (a) shows the computed transmission coefficient as a function of electron energy E. Since the graphene is doped in the experiments, we apply a small shift to the band structure of the graphene to mimic hole doping (Figure 5 (a) red curve) and electron doping (Figure 5 (a) blue curve), where the former is relevant to our experiments. To account for asymmetry in the junction, at finite source-drain voltage, we re-calculate the transmission coefficient at each source drain-voltage to yield the series of finite-bias transmission curves shown in Figure 5 (b), from which we obtain the finite-bias current and the differential conductance shown in Figure 5 (c) and (d) (see SI. 3 for more details).

To obtain the latter, we noted that the work function of gold is greater than that of graphene, so electrons are expected to transfer from the graphene to the BPDT/Au complex. The positively-charged graphene acts like a positive electrostatic gate and lowers the energy levels of the SAM relative to the Fermi energy of gold. This moves the LUMO of the molecules closer to the gold Fermi energy and results in LUMO dominated transport, as also suggested by the analytical model. To account for this shift and the fact that the graphene doping varies over the area of the device, we computed the average of three I-V curves for Fermi energies of the gold in the range 0.6 ± 0.1 eV. The resulting average I-V and dI/dV curves are shown in Figure 5 (c) and (d). The model captures all the essential features of the experimental curves.

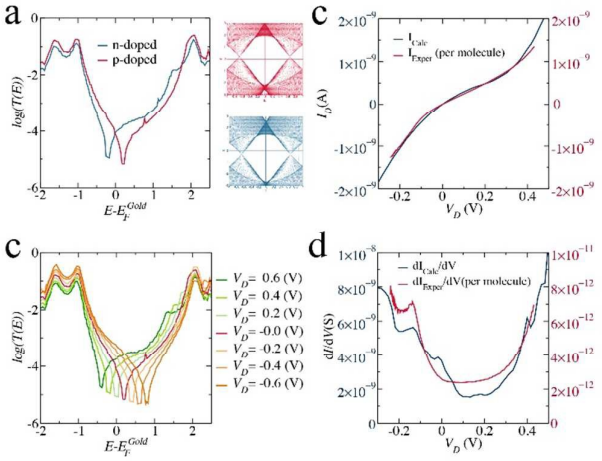

Figure 5. (a) Transport through a SAM with p-doped and n-doped graphene at zero bias voltage with 16 K points in the transverse direction. (b) The logarithm of transmission vs the energy relative to the Fermi energy of gold at various source drain voltages. (c) Comparison between experimental and theoretical current (d) comparison of the average calculated dI/dV for differently doped systems (blue) with the experimental dI/dV (red). The units of conductance and current used in these plots are $G_0 = 2e^2/h$

View Article Online
DOI: 10.1039/C8NR06763E

and $I_0 = 2e/h$. Although the asymmetry and the lowest conductance point in dI/dV curve is similar to the experimental data, the absolute value of the calculated conductance is greater than that of experiment, in common with DFT transport calculations reported in the literature and therefore the vertical axes have been scaled to aid comparison.[37]

4. Conclusion

In summary, the behaviour of cross-plane electron transport through a monolayer graphene/BPDT/Au junction has been investigated using a four-probe measurement. The asymmetric electrical transport characteristics observed in both I-V and dI/dV vs V measurements, arise from the asymmetric structure of the junction, combined with phase-coherent tunneling of electrons from the gold to the graphene via the SAM. These are described using density functional theory and a generic analytic model, which captures the interplay between the energetics of molecular orbitals, the Dirac point of the graphene and inhomogeneity of doping across the area of the graphene electrode.

We have conducted a systematic comparison between single-molecule conductance, the conductance in large area junctions as a function of junction area and combined with DFT modelling and taken together these strongly suggests that the architecture we have proposed here is remarkably successful as a mechanism for making efficient electrical contact to the organic SAMS layer. We estimate that between 10% and 100% of the molecules make electrical contact to the larger area electrodes and that in our smaller junctions, where area scaling and reproducibility is extremely robust this value approaches 100%. These results are encouraging and indicate that graphene/BPDT/Au sandwiches provide an efficient route to electrically contacting SAMS, while preserving cross-plane phase-coherent transport.

Supplementary Information is uploaded separately. The python script for the analytical model is uploaded as "Supplementary Code" in addition to **Supplementary Information**.

Conflicts of interest

There are no conflicts to declare.

Acknowledgements

We thank Dr. Yi Li and Dr. Viktoryia Shautsova for the helpful discussion on the processing of KFM and Raman spectroscopy results. We thanks EPSRC for support through grants EP/N03337X/1 and EP/P027156/1.

Notes

‡ The experimental value of conductance for single molecule between Au and graphene electrodes can be predicted using the calculated ratio,

$$G_M = G^{exp}_{Au/BPDT/Au} \times \frac{G^{Calc}_{graphene/BPDT/Au}}{G^{Calc}_{Au/BPDT/Au}}$$

References

1 Q. Yu, J. Lian, S. Siriponglert, H. Li, Y. P. Chen and S.-S. Pei, Appl Phys Lett 2008, 93, 113103.
2 A. Nitzan and M. A. Ratner, Science 2003, 300, 1384.
3 M. Galperin, M. A. Ratner, A. Nitzan and A. Troisi, Science 2008, 319, 1056.
4 V. Kaliginedi, P. Moreno-García, H. Valkenier, W. Hong, V. M. García-Suárez, P. Buiter, J. L. H. Otten, J. C. Hummelen, C. J. Lambert and T. Wandlowski, J Am Chem Soc, 2012, 134, 5262.
5 D. Xiang, H. Jeong, T. Lee and D. Mayer, Adv Mater 2013, 25, 4845.
6 Y. Liu, L. Yuan, M. Yang, Y. Zheng, L. Li, L. Gao, N. Nerngchamnong, C. T. Nai, C. S. Suchand Sangeeth, Y. P. Feng, C. A. Nijhuis and K. P. Loh, Nat Commun 2014, 5, 5461.
7 D. Z. Manrique, Q. Al-Galiby, W. Hong and C. J. Lambert, Nano Lett 2016, 16, 1308.
8 H. Sadeghi, S. Sangtarash and C. J. Lambert, Nano lett 2015, 15, 7467.
9 C. J. Lambert, H. Sadeghi and Q. H. Al-Galiby, C R Phys 2016, 17, 1084.
10 H. B. Akkerman, P. W. M. Blom, D. M. de Leeuw and B. de Boer, Nature 2006, 441, 69.
11 Y. Jang, H. Jeong, D. Kim, W. T. Hwang, J. W. Kim, I. Jeong, H. Song, J. Yoon, G. Yi, H. Jeong and T. Lee, Nanotechnology 2016, 27, 145301.
12 A. P. Bonifas and R. L. McCreery, Nat Nanotechnol 2010, 5, 612.
13 J.-J. Chen, J. Meng, Y. Zhou, H. Wu, Y. Bie, Z. Liao, D. Yu, Nat Commun 2013, 4, 1921.
14 B. A. Hylke and B. Bert de, J Phys-Condens Mat 2007, 20, 013001.
15 R. L. McCreery and A. J. Bergren, Adv Mater 2009, 21, 4303.
16 C. S. S. Sangeeth, A. T. Demissie, L. Yuan, T. Wang, C. D. Frisbie, and C. A. Nijhuis, J Am Chem Soc 2016, 138, 7305.
17 K. S. Novoselov, D. Jiang, F. Schedin, T. J. Booth, V. V. Khotkevich, S. V. Morozov, A. K. Geim, P Natl Acad Sci USA 2005, 102, 10451.
18 K. I. Bolotin, K. J. Sikes, Z. Jiang, M. Klima, G. Fudenberg, J. Hone, P. Kima, H. L. Stormer, Solid State Commun 2008, 146, 351.
19 A. K. Geim and K. S. Novoselov, Nat Mater 2007, 6, 183.
20 X. Wang, X. Li, L. Zhang, Y. Yoon, P. K. Weber, H. Wang, J. Guo, J. Guo, H. Dai, Science 2009, 324, 768.
21 X. Guo, J. P. Small, J. E. Klare, Y. Wang, M. S. Purewal, I. W. Tam, B. H. Hong, R. Caldwell, L. Huang, S. O'Brien, J. Yan, R. Breslow, S. J. Wind, J. Hone, P. Kim, C. Nuckolls, Science 2006, 311, 356.
22 T. Li, M. Jevric, J. R. Hauptmann, R. Hviid, Z. Wei, R. Wang, N. E. A. Reeler, E. Thyrhaug, S. Petersen, J. A. S. Meyer, N. Bovet, T. Vosch, J. Nygård, X. Qiu, W. Hu, Y. Liu, G. C. Solomon, H. G. Kjaergaard, T. Bjørnholm, M. B. Nielsen, B. W. Laursen, K. Nørgaard, Adv Mater 2013, 25, 4164.
23 S. Seo, M. Min, S. M. Lee and H. Lee, Nat Commun 2013, 4, 1920.
24 J. Prasongkit and A. R. Rocha, RSC Adv 2016, 6, 59299.
25 M. Bürkle, J. K. Viljas, A. Mishchenko, D. Vonlanthen, G. Schön, M. Mayor, T. Wandlowski, F. Pauly, Phys Rev B 2012, 85, 075417.

View Article Online
DOI: 10.1039/C8NR06763E

26 M. S. Inkpen, M. Lemmer, N. Fitzpartrick, D. C. Milan, R. J. Nichols, N. J. Long and T. Albrecht, J Ame Chem Soc 2015, 137, 9971.
27 M. Lemmer, M. S. Inkpen, K. Kornysheva, N. J. Long and T. Albrecht. Nat Commun 2016, 7, 12922.
28 A. Rodriguez and A. Laio. Science 2014, 344, 1492.
29 X. Wang, Z. Liu, M. Zhuang, H. Zhang, X. Wang, Z. Xie, D. Wu, B. Rena, and Z. Tian, App Phys Lett 2007, 91, 101105.
30 J. E. Lee, G. Ahn, J. Shim, Y. S. Lee and S. Ryu, Nat Commun 2012, 3, 1024.
31 M. S. José, E. Artacho, J. D. Gale, A. García, J. Junquera, P. Ordejón and D. Sánchez-Portal, J Phys-Condens Mat 2002, 14, 2745.
32 H. Wolfgang, C. Wang, R. Jitchati, I. Grace, S. Martín, A. S. Batsanov, S. J. Higgins, M. R. Bryce, C. J. Lambert, P. S. Jensen and R. J. Nichols, J Phys-Condens Mat 2008, 20, 374119.
33 A. Mishchenko, D. Vonlanthen, V. Meded, M. Bürkle, C. Li, I. V. Pobelov, A. Bagrets, J. K. Viljas, F. Pauly, F. Evers, M. Mayor, T. Wandlowski, Nano Lett 2009, 10, 156.
34 C. J. Lambert, Chem Soc Rev 2015, 44, 875.
35 G. Bianco, M. Losurdo, M. Giangregorio, P. Capezzuto, G. Bruno, Phys Chem Chem Phys 2014, 16, 3632.
36 G. V. Bianco, M. M. Giangregorio, M. Losurdo, A. Sacchetti, P. Capezzuto, G. Bruno, J Nanomater 2016, 9, 2561326.
37 J. Ferrer, C. J. Lambert, V. M. García-Suárez, D. Z. Manrique, D. Visontai, L. Oroszlany, R. Rodríguez-Ferradás, I. Grace, S. W. D. Bailey, K. Gillemot, H. Sadeghi and L. A. Algharagholy, New J Phys 2014, 16, 093029.

View Article Online
DOI: 10.1039/C8NR06763E

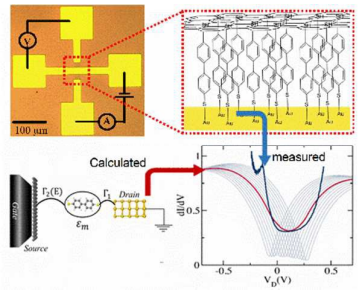

Experimental scalability of junction properties, in combination with theoretical transmission probability, demonstrate a significantly enhanced molecular connection.